

Multiplicity fluctuations near the QCD critical point

M. HIPPERT* and E. S. FRAGA†

*Instituto de Física, Universidade Federal do Rio de Janeiro,
Caixa Postal 68528, 21941-972, Rio de Janeiro, Rio de Janeiro, Brazil*

(Dated: October 14, 2018)

Statistical moments of particle multiplicities in heavy-ion collision experiments are an important probe in the exploration of the phase diagram of strongly interacting matter and, particularly, in the search for the QCD critical end point. In order to appropriately interpret experimental measures of these moments, however, it is necessary to understand the role of experimental limitations, as well as background contributions, providing expectations on how critical behavior should be affected by them. We here present a framework for calculating moments of particle multiplicities in the presence of correlations of both critical and spurious origins. We also include effects from resonance decay and a limited acceptance window, as well as detector efficiency. Although we focus on second-order moments, for simplicity, an extension to higher-order moments is straightforward.

I. INTRODUCTION

The QCD phase diagram in the temperature versus baryonic chemical potential plane is marked by very distinct regimes, characterized by different (approximate) symmetries and degrees of freedom. However, the nature of these regimes and the transitions between them is still not settled. While first-principle calculations face the breakdown of perturbation theory at low and intermediate energy scales and lattice calculations remain limited to relatively low baryon densities, where an analytic crossover is found [1, 2], effective models suggest a first-order phase transition at high densities. The first-order coexistence line, related to the restoration of chiral symmetry, should end at lower densities in a second-order critical end point of unknown location [3–5].

The possibility of experimentally probing this point with current technology and the very peculiar singular behavior associated with a second-order phase transition raise very appealing hopes of accessing reliable information on the main features of the phase diagram of strongly interacting matter, which have motivated considerable experimental and theoretical efforts. The search for the QCD critical point is currently ongoing at the RHIC Beam Energy Scan program [6–8].

On the other hand, notwithstanding its very characteristic features in an ideal scenario, the observation or exclusion of the critical point in the noisy and dynamic context of heavy-ion collision experiments remains an extremely challenging task. Whereas the main probe in the pursuit for such a point is the increase of long-range fluctuations caused by a diverging correlation length in its neighborhood [9–11], the short lifetime and small size of the formed system will considerably limit its growth [12–19]. Moreover, collisions are not perfectly controlled and are affected by initial-state fluctuations, so that spurious sources of fluctuations could possibly hide or mimic

the expected signatures [9, 19–23]. Finally, the medium which is formed in experiments undergoes very fast expansion and cooling, followed by freeze-out and rescattering, which may also have a strong influence upon critical behavior [22, 24–26]. It is thus clear that care should be taken when comparing naive theoretical expectations with actual measurements. Such difficulties call for the use of observables that can serve as robust probes of criticality. The search for reliable signatures demands a correct understanding of both critical fluctuations and relevant background contributions, as well as their dependence on center-of-mass energy, collision centrality and kinematic cuts [16, 21, 27, 28].

In this paper we introduce a simple, yet reasonably general framework for understanding how both critical and background fluctuations affect different fluctuation measures. For that purpose, we adopt a simplified model of long-range fluctuations [3, 9, 19]. We also show how kinematic cuts and effects from resonance decay can be included and how they affect our results. Since we restrict ourselves to equilibrium and isotropy assumptions, we focus on multiplicity fluctuations. This simple framework provides a useful tool for understanding multiplicity fluctuations near the critical point.

The outline of the paper is as follows. In Sec. II, we explain our models for critical and spurious fluctuations and discuss the growth of the correlation length near the critical point. In Sec. III, we describe a method for analytically calculating multiplicity fluctuation measures in an equilibrated gas of quasi-free particles. Sections IV and V discuss effects from a limited acceptance window and resonance decay, respectively. Finally, Sec. VI summarizes our results, while Sec. VII presents final remarks.

II. FLUCTUATIONS NEAR THE CRITICAL POINT

A. Critical fluctuations

Inspired by Refs. [3, 9], we describe critical fluctuations as fluctuations of an order parameter $\sigma(x)$, with a

* hippert@if.ufrj.br

† fraga@if.ufrj.br

probability distribution

$$\mathcal{P}[\sigma] \sim e^{-\Omega[\sigma]/T}, \quad (1)$$

and, for small fluctuations, we approximate the effective free energy $\Omega[\sigma]$ as

$$\Omega[\sigma] \approx \int d^3x \left\{ \frac{1}{2}(\nabla\sigma)^2 + \frac{1}{2}m_\sigma^2 \sigma^2 \right\}, \quad (2)$$

where we have imposed $\langle\sigma\rangle = 0$. The mass m_σ can be shown to be the inverse of the correlation length ξ and vanishes at the critical point, rendering long-wavelength fluctuations essentially costless.

Thus, as the critical point is approached, long-range fluctuations get increasingly strong until, for very small values of $m_\sigma = \xi^{-1}$, they get too large and Eq. (2) loses validity altogether. For the sake of simplicity, since long wavelengths dominate, we look exclusively at fluctuations of $\sigma_0 := \int d^3x \sigma(x)/V$. Integrating over shorter wavelengths in (1) allows us to define a probability distribution for σ_0 ,

$$P(\sigma_0) \sim e^{-\frac{V}{T} \frac{m_\sigma^2}{2} \sigma_0^2}. \quad (3)$$

Non-Gaussian fluctuations, which are important probes in the search for the critical point, can be described by including in (2) terms of higher order in σ , which would also extend the validity of the model [3].

Equation (3) describes global fluctuations of the order parameter in equilibrium in some region of the phase diagram around the critical end point where fluctuations are not too large and a classical treatment for the order parameter is valid. It neglects dynamical effects which might make global correlations unattainable in the relevant time scales and provides only a crude model. However, this simplification enables us to make both simulations and analytical calculations in a relatively simple fashion, even in the case of non-Gaussian fluctuations, providing an optimistic, yet valuable tool for understanding how different effects affect critical fluctuations. The off-equilibrium evolution of the order parameter is tackled, for instance, in Refs. [12, 17, 18, 22].

A connection with observables requires coupling the order parameter to particle fields. We consider linear couplings in σ_0 which enter the Lagrangian as mass corrections for both protons and pions,

$$\mathcal{L}_{int} = G \sigma_0 \vec{\pi} \cdot \vec{\pi} + g \sigma_0 \bar{\psi}_p \psi_p, \quad (4)$$

where the value of G can be estimated as ~ 300 MeV near the critical point by symmetry arguments [9], but only the vacuum value of $g \sim 10$ is known, from the linear sigma model [29].

In the absence of reliable information on its value as a function of collision energy or temperature and chemical potential, we treat $\xi = m_\sigma^{-1}$ as an input to our calculations. This correlation length, whose size determines the strength of the fluctuations [3, 9], is not determined

solely by an equilibrium equation of state or static universality class exponents, but is also influenced by both finite-size effects and dynamics, with the latter being expected to dominate [12]. We consider limitations to the growth of ξ from critical slowing down as discussed in Ref. [12], with the evolution of $\xi(t)$ in the proper-time t given by the ansatz equation

$$\frac{d\xi}{dt} = A \left(\frac{\xi}{\xi_0} \right)^{2-z} \left(\frac{\xi_0}{\xi} - \frac{\xi_0}{\xi_{eq}(t)} \right), \quad (5)$$

where $\xi_{eq}(t) = \xi_0 |t/\tau|^{-\nu/\beta\delta}$ and $\alpha = 0.11$, $\nu = 0.63$, $z = 2 + \alpha/\nu$, $\beta = 0.326$ and $\delta = 4.80$, coming from universality class arguments [30–32]. The nonuniversal dimensionless parameter A cannot be directly estimated, but is limited by causality, depending on the combination $x = \tau/\xi_0$, where τ defines a cooling time scale and ξ_0 is the typical value of the correlation length at which universal behavior sets in [19]. However, we believe our previous estimate for the time spent in the critical region, $\tau = 5.5$ fm, to be overly optimistic, comparable to the lifetime of the system [19]. This parameter strongly influences the maximum value of ξ/ξ_0 , which depends on the combination $Ax \leq 1.3x^{1.33}$. Taking the more conservative, but still optimistic value of $\tau = 1$ fm yields, for $\xi_0 = 1.6$ fm, a maximum value of $\xi/\xi_0 = 1.3$, instead of the previous maximum of $\xi/\xi_0 = 1.9$.

Apart from the different value of τ , the treatment described here is the same as in Ref. [19], where some of its aspects are discussed in more detail and the distribution (3) is used to build a simple Monte Carlo implementation of critical fluctuations to which background contributions can be superposed.

B. Background fluctuations

One of the most challenging limitations in the search for fluctuations which might serve as a probe of criticality is understanding the role and behavior of background contributions. These contributions may come from any source of undesired statistical correlation, including quantum statistics, fluctuations of imperfectly controlled thermodynamic parameters, such as temperature and system size, and correlations from initial conditions [9, 19–23, 33]. An experimental discovery of the critical point can hardly be claimed before background is either controlled, well described in terms of beam energy dependence or eliminated by a good choice of signatures.

We use the same model for spurious fluctuations as in Ref. [19]. For temperature fluctuations we simply take a Gaussian distribution of 5% width. For volume fluctuations, we take a probability distribution $\mathcal{P}_b(b) \propto b$ for the impact parameter b , and suppose the final volume V to be proportional to the initial overlap area \mathcal{A} between the two nuclear disks of radius R_N , with a proportionality

constant C ,

$$\begin{aligned} V(b, R_N) &= C \mathcal{A}(b, R_N) \\ &= 2C R_N^2 \cos^{-1} \left(\frac{b}{2R_N} \right) - b \sqrt{R_N^2 - \frac{b^2}{4}}, \end{aligned} \quad (6)$$

in which we take $R_N = r_0 = 6.38$ fm for gold nuclei (see Refs. [34, 35]) and C can be fixed by the average radius, or average volume, of the system at freeze-out. This model enables us to find the system-volume distribution in a given centrality range, while disregarding initial-state fluctuations and other effects [23].

These are very crude models for background fluctuations, but more complete models can be very straightforwardly included within the present framework. Volume fluctuations have previously been considered in Refs. [23, 33, 36, 37], as well as the methods for partially correcting them in data analysis [23, 33]. Certain fluctuation measures, called strongly intensive, are, by construction, insensitive to such fluctuations [20, 37].

III. COMPUTING FLUCTUATIONS FROM ENERGY-LEVEL SHIFTS

A. Methodology

Besides simulating fluctuations using Monte Carlo techniques [19], it is possible to derive analytical expressions for signatures of the critical point within this scenario. We now develop a scheme to calculate observables in the presence of spurious and critical fluctuations. It has the advantage of naturally including finite-size effects.

Inspired by Sec. II A, we note that a fluctuation of the order parameter σ_0 , produces a shift in each single-particle energy level ω ,

$$\begin{aligned} \omega &= \sqrt{p^2 + m_0^2 + \delta m^2} \\ &\approx \omega_0 \left[1 + \frac{1}{2} \frac{\delta m^2}{\omega_0^2} - \frac{1}{8} \frac{(\delta m^2)^2}{\omega_0^4} + \dots \right] \\ &\approx \omega_0 \left[1 + \frac{m \delta m}{\omega_0^2} + \frac{1}{2} \left(1 - \frac{m^2}{\omega_0^2} \right) \frac{(\delta m)^2}{\omega_0^2} + \dots \right], \end{aligned} \quad (7)$$

where $\delta m = g \delta \sigma$ is the corresponding mass correction and ω_0 is the original one-particle energy.

Spurious fluctuations of parameters such as volume, temperature and chemical potential can also be described as energy-level shifts. Suppose we have a gas of free particles confined to a typical length scale R . For both cubic and spherically symmetric boundary conditions, the allowed momentum levels will be distributed depending on the value of R , $p_i = \alpha_i/R$, where α_i represents constants which depend on the boundary conditions. A small change δR in the size of the system, hence, modifies the momenta, p_i , and the one-particle energies, ω_i , of the

allowed modes,

$$p_i = \frac{\alpha_i}{R + \delta R} \approx p_{0i} \left[1 - \frac{\delta R}{R} + \left(\frac{\delta R}{R} \right)^2 + \dots \right], \quad (8)$$

$$\begin{aligned} \omega_i &= \sqrt{p_i^2 + m^2} \approx \omega_{0i} \left\{ 1 - \left(\frac{p_{0i}}{\omega_{0i}} \right)^2 \frac{\delta R}{R} + \right. \\ &\quad \left. + \frac{1}{2} \left[3 \left(\frac{p_{0i}}{\omega_{0i}} \right)^2 - \left(\frac{p_{0i}}{\omega_{0i}} \right)^4 \right] \left(\frac{\delta R}{R} \right)^2 + \dots \right\}. \end{aligned} \quad (9)$$

Temperature and chemical potential fluctuations can be included in a similar fashion. All the quantities we calculate in this work depend on temperature, chemical potential and energy levels only through the Boltzmann factor $e^{-(\omega_i - \mu)/T}$. As a consequence, fluctuations of both temperature and chemical potential are equivalent to fluctuations of the energy levels. For a fluctuation δT in the temperature, for instance,

$$\frac{\omega_{0i} - \mu}{T + \delta T} = \frac{\omega_{0i} - \mu}{T} \left(1 - \frac{\delta T}{T} + \frac{\delta T^2}{T^2} + \dots \right), \quad (10)$$

so it is equivalent to a fluctuation in ω_i of the form

$$\delta \omega_i^T = (\omega_{0i} - \mu) \left(-\frac{\delta T}{T} + \frac{\delta T^2}{T^2} + \dots \right). \quad (11)$$

For a fluctuation $\delta \mu$ in the chemical potential,

$$\omega_{0i} - (\mu + \delta \mu) = \omega_{0i} + \delta \omega_i^\mu - \mu, \quad (12)$$

with $\delta \omega_i^\mu = -\delta \mu$.

In order to calculate the effect of these fluctuating energy shifts, an ensemble of different $(\delta \sigma, \delta R, \delta T, \delta \mu, \dots)$ and occupation numbers, $\{n_i\}$, can be considered. Furthermore, configurations in this ensemble can be organized according to the values of δR and $\delta \sigma$, so that averages can be calculated by first averaging over a regular grand-canonical ensemble for a fixed $(\delta \sigma, \delta R, \delta T, \delta \mu, \dots)$ (denoted by $\langle \dots \rangle$) and then averaging over $(\delta \sigma, \delta R, \delta T, \delta \mu, \dots)$ (denoted by $\overline{\dots}$).

We proceed by expanding the first averages, $\langle \dots \rangle$, as power series in $\delta \sigma, \delta R, \dots$ before averaging over their different values. Defining $\overline{\delta \sigma} = \overline{\delta R} = \overline{\delta T} = \overline{\delta \mu} = 0$, an expansion to at least order $(\delta \omega)^2$ in the single-particle energy corrections is necessary for consistency.

B. Second-order expansion

We now turn to the actual calculations. The lowest-order contributions to observables come from the variance of each fluctuating quantity, $\overline{\delta \sigma^2}$, $\overline{\delta R^2}$ and so on, corresponding to a Gaussian approximation. Before we go further, it is useful to introduce some relations, which

can be derived from $\partial^n(\beta F)/\partial\zeta_i^n = \langle(\Delta n_i)^n\rangle$:

$$\begin{aligned}\langle n_i \rangle &= f(\zeta_i) := (e^{-\zeta_i} \mp 1)^{-1}, \\ \langle(\Delta n_i)^2\rangle &= f'(\zeta_i) = f(\zeta_i) (1 \pm f(\zeta_i)), \\ \langle(\Delta n_i)^3\rangle &= f''(\zeta_i) = f'(\zeta_i) (1 \pm 2f(\zeta_i)), \\ \langle(\Delta n_i)^4\rangle &= f'''(\zeta_i) = f'(\zeta_i)(1 \pm 6f'(\zeta_i)),\end{aligned}\quad (13)$$

where $\Delta n_i := n_i - \langle n_i \rangle$, F is the free-energy, $\beta := 1/T$, $\zeta_i := -\beta(\omega_i - \mu)$ and the upper (lower) sign stands for bosons (fermions).

We start by the average occupation number of the i th energy level. Expanding the ordinary expression for the grand-canonical ensemble up to $\delta\omega_i^2$, for noninteracting particles,

$$\begin{aligned}\langle n_i \rangle &\approx f(\zeta_{0i}) - \beta f'(\zeta_{0i}) \delta\omega_i + \\ &+ \frac{\beta^2}{2} f''(\zeta_{0i}) (\delta\omega_i)^2 + \dots,\end{aligned}\quad (14)$$

and taking the average over fluctuations of the induced shifts,

$$\begin{aligned}\overline{\langle n_i \rangle} &\approx f(\zeta_{0i}) - \beta f'(\zeta_{0i}) \overline{\delta\omega_i} + \\ &+ \frac{\beta^2}{2} f''(\zeta_{0i}) \overline{(\delta\omega_i)^2} + \dots,\end{aligned}\quad (15)$$

where $\zeta_{0i} := -\beta(\omega_{0i} - \mu_0)$.

A calculation of the microscopic correlator¹ [9] is also possible,

$$\begin{aligned}\overline{\langle \Delta n_i \Delta n_j \rangle} &:= \overline{\langle n_i n_j \rangle} - \overline{\langle n_i \rangle} \overline{\langle n_j \rangle} \\ &= \langle n_i \rangle \langle n_j \rangle - \overline{\langle n_i \rangle} \overline{\langle n_j \rangle} + \delta_{ij} \overline{f'(-\beta\omega_i)}.\end{aligned}\quad (16)$$

From Eq. (15), since $\overline{\delta\omega_i \delta\omega_j} \sim \mathcal{O}(\delta\sigma^4, \delta R^4, \dots)$,

$$\begin{aligned}\overline{\langle \Delta n_i \Delta n_j \rangle} &\approx f'(\zeta_{0i}) f'(\zeta_{0j}) \beta^2 \overline{\delta\omega_i \delta\omega_j} + \\ &+ \delta_{ij} \left(f'(\zeta_{0i}) - \beta f''(\zeta_{0i}) \overline{\delta\omega_i} + \right. \\ &\quad \left. + \frac{\beta^2}{2} f'''(\zeta_{0i}) \overline{(\delta\omega_i)^2} \right),\end{aligned}\quad (17)$$

where derivatives of $f(\zeta_i)$ can be extracted from Eq. (13) and we have used that $\langle \Delta n_i \Delta n_j \rangle = \delta_{ij} \langle (\Delta n_i)^2 \rangle$ for free particles.

Finally, from Eqs. (7), (9), (11) and (12), neglecting terms of order $(\delta\sigma \delta R)^2$, for instance, and assuming independent fluctuations,²

$$\begin{aligned}\overline{\delta\omega_i} &\approx \frac{\omega_{0i}}{2} \left[3 \left(\frac{p_{0i}}{\omega_{0i}} \right)^2 - \left(\frac{p_{0i}}{\omega_{0i}} \right)^4 \right] \overline{\left(\frac{\delta R}{R} \right)^2} + \\ &+ \frac{g^2}{2\omega_{0i}} \left(1 - \frac{m^2}{\omega_{0i}^2} \right) \overline{(\delta\sigma)^2} + (\omega_{0i} - \mu) \overline{\left(\frac{\delta T}{T} \right)^2},\end{aligned}\quad (18)$$

$$\begin{aligned}\overline{\delta\omega_i \delta\omega_j} &\approx \frac{g^2 m^2}{\omega_{0i} \omega_{0j}} \overline{(\delta\sigma)^2} - \frac{(p_{0i} p_{0j})^2}{\omega_{0i} \omega_{0j}} \overline{\left(\frac{\delta R}{R} \right)^2} \\ &+ (\omega_{0i} - \mu)(\omega_{0j} - \mu) \overline{\left(\frac{\delta T}{T} \right)^2} + \overline{(\delta\mu)^2}.\end{aligned}\quad (19)$$

The average and variance of the particle multiplicity can then be written as

$$\overline{\langle N \rangle} = \sum_i \overline{\langle n_i \rangle},\quad (20)$$

$$\overline{\langle (\Delta N)^2 \rangle} = \sum_{i,j} \overline{\langle \Delta n_i \Delta n_j \rangle}.\quad (21)$$

The results presented above can be generalized to other observables and higher-order moments, by including higher orders of $\delta\omega$. Since volume fluctuations modify the momentum modes, the calculation of fluctuation measures involving the momenta requires the computation of terms such as $p_i \langle \Delta n_i \Delta n_j \rangle$ and $p_i p_j \langle \Delta n_i \Delta n_j \rangle$, for instance.

C. Hard-sphere boundary conditions

The finite size of the system requires the specification of boundary conditions in order to use results from Sec. III B. We choose to work with Dirichlet boundary conditions on a sphere of radius R ,

$$\Phi(R, \theta, \phi) = 0.\quad (22)$$

Although they are not very realistic, these boundary conditions are more natural than cubic ones and yet fairly simple.

The eigenstates of the squared momentum p^2 in a spherical geometry are given by the spherical Bessel functions of the first kind $j_\ell(pr)$, where the orbital angular momentum ℓ is a positive integer. The allowed eigenvalues of p are given by $p_i^{(\ell)} = \alpha_i^{(\ell)}/R$, where $\alpha_i^{(\ell)}$ is the i th root of $j_\ell(x)$, $j_\ell(\alpha_i^{(\ell)}) = 0$. For each pair (ℓ, i) there are $2\ell + 1$ linearly independent one-particle quantum states, corresponding to eigenvalues of the z component of the angular momentum $-\ell \leq m \leq \ell$.

In the absence of kinematic cuts,

$$\begin{aligned}\overline{\langle (\Delta N)^2 \rangle} &= \sum_{\substack{\ell_1, m_1, i_1 \\ \ell_2, m_2, i_2}} \overline{\langle \Delta n_{\ell_1, i_1} \Delta n_{\ell_2, i_2} \rangle} \\ &= \sum_{\substack{\ell_1, i_1 \\ \ell_2, i_2}} (2\ell_1 + 1)(2\ell_2 + 1) A_{(\ell_1, i_1), (\ell_2, i_2)} + \\ &+ \sum_{\ell_1, i_1} (2\ell_1 + 1) B_{(\ell_1, i_1)},\end{aligned}\quad (23)$$

where, from Eq. (17),

$$\begin{aligned}A_{(\ell_1, i_1), (\ell_2, i_2)} &= f'(\zeta_{0(\ell_1, i_1)}) f'(\zeta_{0(\ell_2, i_2)}) \times \\ &\quad \times \beta^2 \overline{\delta\omega_{(\ell_1, i_1)} \delta\omega_{(\ell_2, i_2)}},\end{aligned}\quad (24)$$

¹ When in an overlined expression, $\Delta n_i := n_i - \overline{\langle n_i \rangle}$.

² It is, of course, very straightforward to relax this assumption, provided the relevant correlations.

$$B_{(\ell,i)} = f'(\zeta_0(\ell_1, i_1)) - \beta f''(\zeta_0(\ell_1, i_1)) \overline{\delta\omega_{(\ell_1, i_1)}} + \frac{\beta^2}{2} f'''(\zeta_0(\ell_1, i_1)) \overline{(\delta\omega_{(\ell_1, i_1)})^2}. \quad (25)$$

It is also possible to calculate moments involving different kinds of particles, A and B , such as $\langle \Delta N^A \Delta N^B \rangle$, for instance. In this case, the previous calculations apply with small modifications and we have, in Eq. (23),

$$A_{(\ell_1, i_1), (\ell_2, i_2)} = f'_A(\zeta_0^A(\ell_1, i_1)) f'_B(\zeta_0^A(\ell_2, i_2)) \times \beta^2 \overline{\delta\omega_{(\ell_1, i_1)}^A \delta\omega_{(\ell_2, i_2)}^B}, \quad (26)$$

$$B_{(\ell,i)} = 0, \quad (27)$$

where Eq. (19) can be used with adaptations for the chemical potentials, masses and couplings.

IV. ACCEPTANCE CUTS

Expression (23) is valid for the total multiplicity of particles under the chosen boundary conditions. Experimentally, however, only the particles produced in a certain range of transverse momentum and pseudorapidity are detected and used in data analysis. The behavior of fluctuation measures under variations of these acceptance cuts has been discussed, for example, in Refs. [27, 28, 38–40]. Here we show how they can be included in our framework.

The quantum numbers ℓ and p , chosen in Sec. III C, give us no information about the separate longitudinal and transverse parts of the momentum. However, it is possible to calculate the fraction of particles of a given momentum p which will be in the selected window of rapidity and transverse momentum, assuming their momenta are distributed isotropically and without angular correlation. Because of quantum statistics, this assumption is not obviously true for indistinguishable particles, but should hold as a reasonable approximation.

The upper and lower transverse momentum cuts, $p_T \leq p_+$ and $p_T \geq p_-$, may be written as

$$u^2 \geq 1 - \left(\frac{p_+}{p}\right)^2, \quad u^2 \leq 1 - \left(\frac{p_-}{p}\right)^2. \quad (28)$$

where $u := \cos\theta$, $p_T := p|\sin\theta|$ and θ is the angle between the momentum of the particle and the beam axis.

We also select a window for the pseudorapidity $\eta = \ln[(p+p_z)/(p-p_z)]/2$. Since $\eta = \ln[(1+u)/(1-u)]/2$, $|\eta| \leq \eta_C$ yields

$$e^{-2\eta_C} \leq \frac{1+u}{1-u} \leq e^{2\eta_C}, \quad (29)$$

resulting in

$$e^{-2\eta_C} - 1 \leq u(1+e^{-2\eta_C}) \quad u(1+e^{2\eta_C}) \leq e^{2\eta_C} - 1, \quad (30)$$

$$|u| \leq \tanh \eta_C. \quad (31)$$

Combining both rapidity and transverse momentum cuts, we have

$$\max\left[0, \frac{p^2 - p_+^2}{p^2}\right] \leq u^2 \leq \min\left[\frac{p^2 - p_-^2}{p^2}, \tanh^2 \eta_C\right]. \quad (32)$$

Since we assume an uncorrelated and uniform angular distribution of particles and $|u|$ is uniformly distributed in the interval $(0, 1]$, the resulting fraction of accepted particles is

$$F(p) = \int_{\Omega_{\text{acc}}(p)} \frac{d\Omega}{4\pi} = \max[u_{\text{max}}(p) - u_{\text{min}}(p), 0], \quad (33)$$

where

$$u_{\text{max}}(p) = \begin{cases} \min\left[\sqrt{\frac{p^2 - p_-^2}{p^2}}, \tanh \eta_C\right] & p > p_- \\ 0 & p < p_- \end{cases}, \quad (34)$$

$$u_{\text{min}}(p) = \begin{cases} \sqrt{\frac{p^2 - p_+^2}{p^2}} & p > p_+ \\ 0 & p < p_+ \end{cases}. \quad (35)$$

A plot of $F(p)$ for different acceptance windows is shown in Fig. 1.

Event-by-event cumulants of observables may now be calculated. Attention should be drawn to the fact that the acceptance of particles is probabilistic and follows a binomial distribution, which also contributes to fluctuations. Hence, denoting as $\langle \dots \rangle_{\text{acc}}$ an average over accepted particles only, for a single value of p ,

$$\langle n_p \rangle_{\text{acc}} = F(p) \langle n_p \rangle, \quad (36)$$

$$\langle n_p^2 \rangle_{\text{acc}} = \langle n_p F(p) + n_p(n_p - 1) F(p)^2 \rangle, \quad (37)$$

with which,

$$\overline{\langle (\Delta n_p)^2 \rangle}_{\text{acc}} = \overline{F(p)^2 \langle n_p^2 \rangle} - \left(\overline{F(p) \langle n_p \rangle}\right)^2 + \overline{F(p)(1 - F(p)) \langle n_p \rangle}, \quad (38)$$

where we denote $\Delta n_p := n_p - \langle n_p \rangle_{\text{acc}}$ or $\Delta n_p := n_p - \overline{\langle n_p \rangle}_{\text{acc}}$ in the corresponding averages over accepted particles.

For the sake of simplicity, we neglect fluctuations of $F(p)$. For midrapidity, $F(p)$ is only sensitive to p in the limits of the acceptance region, as seen in Fig. 1, and fluctuations of p should only be relevant for the acceptance probability in these narrow regions. In this approximation,

$$\overline{\langle (\Delta n_p)^2 \rangle}_{\text{acc}} = F(p_0)^2 \overline{\langle (\Delta n_p)^2 \rangle} + F(p_0)(1 - F(p_0)) \overline{\langle n_p \rangle}, \quad (39)$$

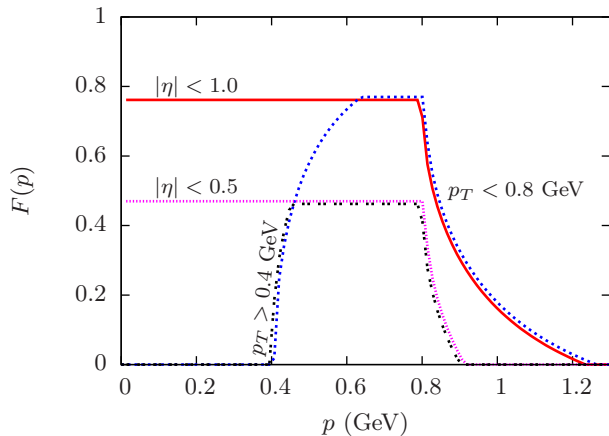


FIG. 1. Particle acceptance probability or fraction as a function of its momentum p for isotropic emission. We display curves corresponding to $|\eta| < 1.0$, $|\eta| < 0.5$ and $p_T > 0$, $p_T > 0.4$ GeV, with $p_T < 0.8$ GeV for all of the curves. Lines were slightly shifted to avoid superposition.

where p_0 is the unperturbed value of the momentum mode in question. A similar result is found for the correlator of different momentum modes, while lacking the second term in Eq. (39).

Hence, Eq. (23) is modified to

$$\begin{aligned} \overline{\langle (\Delta N)^2 \rangle} &= \sum_{\substack{\ell_1, m_1, i_1 \\ \ell_2, m_2, i_2}} \overline{\langle \Delta n_{\ell_1, i_1} \Delta n_{\ell_2, i_2} \rangle}_{\text{acc}} \\ &= \sum_{\substack{\ell_1, i_1 \\ \ell_2, i_2}} (2\ell_1 + 1) F(p_{i_1}^{(\ell_1)}) (2\ell_2 + 1) F(p_{i_2}^{(\ell_2)}) A_{(\ell_1, i_1), (\ell_2, i_2)} + \\ &\quad + \sum_{\ell, i_1} (2\ell + 1) \left[F(p_i^{(\ell)})^2 B_{(\ell, i)} + \right. \\ &\quad \left. + F(p_i^{(\ell)}) (1 - F(p_i^{(\ell)})) C_{(\ell, i)} \right], \quad (40) \end{aligned}$$

where $A_{(\ell_1, i_1), (\ell_2, i_2)}$ and $B_{(\ell, i)}$ are given by Eqs. (24) and (25) and $C_{(\ell, i)}$ is found from Eq. (15),

$$\begin{aligned} C_{(\ell, i)} &= f(\zeta_0(\ell, i)) - \beta f'(\zeta_0(\ell, i)) \overline{\delta\omega(\ell, i)} + \\ &\quad + \frac{\beta^2}{2} f''(\zeta_0(\ell, i)) \overline{(\delta\omega(\ell, i))^2} + \dots \quad (41) \end{aligned}$$

As in Ref. [27], we use a probabilistic description for acceptance effects. However, we take into account the momentum dependence in the relevant probabilities. A similar treatment will be applied to resonance decay under acceptance cuts in the next section. Note that a finite detection efficiency $e_0(p)$ can be introduced by making $F(p) \rightarrow e_0(p) \cdot F(p)$.

The implementation of kinematic cuts in our Monte Carlo simulations is far simpler and can be done by independently sampling the momentum direction for each of the produced particles and applying the cuts, also relying

on the assumption of uncorrelated, isotropic emission. It is also straightforward to include the effects of a finite efficiency.

V. RESONANCE DECAY EFFECTS

So far, we have only considered direct particles from a thermal distribution. However, a non-negligible fraction of the final-state particles in a collision come from the decay of unstable particles. In this section, we consider the role of resonance decay in multiplicity fluctuations. The impact of resonance decay in fluctuation measures was previously explored in Refs. [21, 39, 41–45], among others.

We consider particles coming from resonance decay to be affected by spurious fluctuations, but not by critical ones, such that they are expected to dilute signatures of criticality. Moreover, both the decay of unstable particles and the detection of its products in the relevant acceptance window are probabilistic processes, which affects fluctuations of the particle multiplicities.

Resonance decay contributions to particle multiplicity fluctuations can be incorporated to our calculations by using the probability of having each decay product in the acceptance window. These probabilities are computed in Sec. V A and later used in Sec. V B to calculate the desired contributions. Unlike most previous calculations of resonance decay effects, we apply acceptance cuts to the decay products themselves, not to the resonances. For simplicity, we neglect the widths of the resonances. As an example, we apply our methods to the decay of a ρ meson into two pions.

A. Probabilistic treatment

We aim to calculate the distribution of decay products found within the acceptance window. Information about both the average fraction of accepted particles and the corresponding fluctuations is necessary. We limit ourselves to two-particle decays and start with branching ratios of 100%. We use the associated phase-space volume as a measure of probability for the kinematic variables.

We denote the momentum of the resonance by \mathbf{p}_{in} . Since we assume spherical symmetry, there is no preferred direction for it. The products of the decay have momenta \mathbf{p}_1 and \mathbf{p}_2 , with orientations given by polar and azimuthal angles of θ_1, θ_2 and ϕ_1, ϕ_2 , respectively. Imposing energy and momentum conservation, the two-particle phase-space volume differential reads

$$\begin{aligned} d\Phi_{2P} &\sim \frac{p_1^2 dp_1 d\Omega_1}{2 E_1} \frac{p_2^2 dp_2 d\Omega_2}{2 E_2} \delta(E_1 + E_2 - E_{in}) \times \\ &\quad \times \int_{4\pi} d\Omega_{in} \delta^{(3)}(\mathbf{p}_1 + \mathbf{p}_2 - \mathbf{p}_{in}), \quad (42) \end{aligned}$$

where $E_i := \sqrt{p_i^2 + m_i^2}$ and we integrate the direction of the resonance momentum over the whole sphere.

Changing variables from θ_2, ϕ_2 to $\theta_2^{(1)}, \phi_2^{(1)}$, defined with their zenith in \mathbf{p}_1/p_1 ,

$$\begin{aligned} \int_{4\pi} d\Omega_{in} \delta^{(3)}(\mathbf{p}_1 + \mathbf{p}_2 - \mathbf{p}_{in}) &= \frac{1}{p_{in}^2} \delta(|\mathbf{p}_1 + \mathbf{p}_2| - p_{in}) \\ &= \frac{1}{p_{in} p_1 p_2} \delta(\cos \theta_2^{(1)} - \cos \theta^*) \end{aligned} \quad (43)$$

with $\cos \theta^* := (p_{in}^2 - p_1^2 - p_2^2)/2 p_1 p_2$. Hence, using $dE_i/dp_i = p_i/E_i$,

$$\begin{aligned} d\Phi_{2P} &\sim \frac{1}{p_{in}} d\phi_2^{(1)} d\phi_1 d(\cos \theta_1) dE_1 \times \\ &\quad \times dE_2 \delta(E_2 - E_{in} + E_1) \times \\ &\quad \times d(\cos \theta_2^{(1)}) \delta(\cos \theta_2^{(1)} - \cos \theta^*). \end{aligned} \quad (44)$$

If we interpret $d\Phi_{2P}$ as proportional to a probability density, Eq. (44) suggests $\phi_2^{(1)}, \phi_1, \cos \theta_1$ and E_1 to be uniformly distributed among their full range of values, while E_2 and $\theta_2^{(1)}$, the angle between \mathbf{p}_1 and \mathbf{p}_2 , are determined by the former. Notice that the conditions that $E_2^* := E_{in} - E_1$ and $\cos \theta^*$ fall within the integration regions for E_2 and $\cos \theta_2^{(1)}$ implicitly limit the possible values of E_1 . The constraint $\cos^2 \theta^*|_{p_2=p_2^*} \leq 1$, for example, yields

$$E_0 - \frac{1}{2} \Delta E \leq E_1 \leq E_0 + \frac{1}{2} \Delta E, \quad (45)$$

with

$$E_0 := \frac{m_{in}^2 + m_1^2 - m_2^2}{m_{in}^2} \frac{E_{in}}{2}, \quad (46)$$

$$\Delta E := \frac{p_{in}}{m_{in}^2} \sqrt{(m_{in}^2 - m_1^2 - m_2^2)^2 - 4 m_1^2 m_2^2}. \quad (47)$$

It is now possible to sample the number of decay products inside the acceptance window for a resonance of momentum p_{in} . We sample $\phi_2^{(1)}, \phi_1, \cos \theta_1$ and E_1 uniformly and calculate E_2 and $\cos \theta_2^{(1)}$, counting the rate of acceptance within kinematic cuts to find the probability of accepting each particle.³ Results are exemplified in Fig. 2. Condition (45), together with the form of $F(p)$ (see Fig. 1), is responsible for the acceptance probabilities in Fig. 2 vanishing both above $p_{res} \approx 25$ GeV and below $p_{res} \approx 80$ MeV.⁴

In Monte Carlo simulations, the momenta of the decay products can be sampled according to the above scheme for each single resonance.

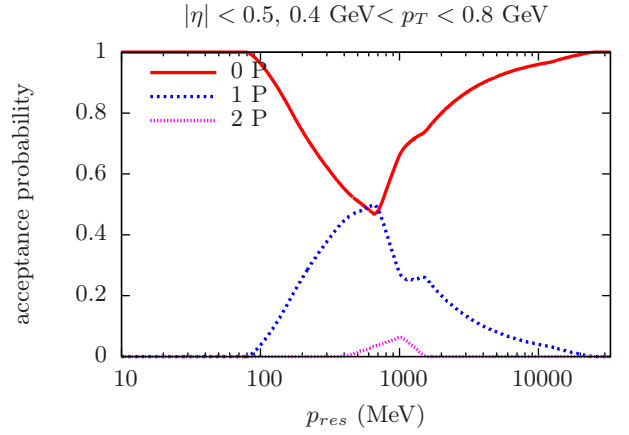


FIG. 2. Probability of accepting 0, 1 or 2 of the two identical particles of mass $m = 140$ MeV coming from the decay of a resonance of mass 770 MeV, with kinematic cuts $0.4 \text{ GeV} < p_T < 0.8 \text{ GeV}$, $|\eta| < 0.5$.

B. Fluctuations from resonance decays

We now apply the results from Sec. V A in the context of particle multiplicity fluctuations. Consider the decay of a resonance R into two distinct particles, A and B , with probabilities P_A, P_B, P_2 and P_0 that only particle A , only particle B , both particles or neither of them are within the acceptance window, respectively. These probabilities provide all the relevant information for the study of multiplicity fluctuations. Then, we calculate averages involving the number of accepted particles, n_l , where $l = A, B$. For the decay of a single resonance with momentum p , for instance, n_l is either 0 or 1 and⁵

$$\langle (n_l)^m \rangle_{\text{kin}} = P_l + P_2, \quad (48)$$

$$\langle (n_A n_B)^m \rangle_{\text{kin}} = P_2, \quad (49)$$

where $m \in \mathbb{N}$ and $\langle \dots \rangle_{\text{kin}}$ denotes an average over the angular distribution of particles within kinematic cuts. For two different decays, i and j , of resonances with the same momentum p ,

$$\langle n_l^{(i)} n_{l'}^{(j)} \rangle_{\text{kin}} = (P_l + P_2)(P_{l'} + P_2). \quad (50)$$

Considering now the independent decays of n_p^R resonances of momentum p , summing over p and taking averages over thermodynamic, critical and spurious fluctuations yields for the contribution from correlations among resonance decay products:

$$\overline{\langle n_l \rangle}_R = \sum_p \overline{\langle n_p^R \rangle} (P_l + P_2), \quad (51)$$

³ The change of variables $\theta_2, \phi_2 \Rightarrow \theta_2^{(1)}, \phi_2^{(1)}$ can be undone by a simple rotation.

⁴ We thank V. Koch for pointing out that these probabilities should vanish at high p_{res} .

⁵ For simplicity of notation, we choose to hide the dependence on p of P_l, P_2, P_0 and kinematic averages.

$$\begin{aligned} \overline{\langle (\Delta n_l)^2 \rangle}_{R,R} &= \sum_{p,p'} \overline{\langle \Delta n_p^R \Delta n_{p'}^R \rangle} (P_l + P_2)(P_l' + P_2') + \\ &+ \sum_p \overline{\langle n_p^R \rangle} (P_l + P_2)(1 - P_l - P_2). \end{aligned} \quad (52)$$

$$\begin{aligned} \overline{\langle \Delta n_A \Delta n_B \rangle}_{R,R} &= \sum_{p,p'} \overline{\langle \Delta n_p^R \Delta n_{p'}^R \rangle} (P_A + P_2)(P_B' + P_2') + \\ &+ \sum_p \overline{\langle n_p^R \rangle} [P_2 - (P_A + P_2)(P_B + P_2)], \end{aligned} \quad (53)$$

As in Sec. IV, we neglect the influence of fluctuations on the fraction of accepted particles, taking the acceptance probability for the unperturbed resonance momentum.⁶ Such effects are present in the full simulations. For the contributions from correlations between resonance decay products and direct particles:

$$\overline{\langle \Delta n_l \Delta n_{l'} \rangle}_{R,\text{dir}} = \sum_p \overline{\langle \Delta n_p^R \Delta n_{l'} \rangle} (P_l + P_2). \quad (54)$$

Contributions from correlations between decays of different resonances can also be calculated in a straightforward fashion.

A similar treatment can be applied to decays into two identical particles, with $P_A = P_B = P_1$, in which case, for a single decay, n_l is either 0, 1 or 2 and

$$\langle (n_A)^m \rangle_{\text{kin}} = P_1 + 2^m P_2, \quad (55)$$

$$\overline{\langle n_A \rangle}_R = \sum_p \overline{\langle n_p^R \rangle} (P_1 + 2 P_2), \quad (56)$$

$$\overline{\langle \Delta n_l \Delta n_{l'} \rangle}_{R,\text{dir}} = \sum_p \overline{\langle \Delta n_p^R \Delta n_{l'} \rangle} (P_1 + 2 P_2), \quad (57)$$

and Eqs. (52) and (53) are combined into a single result,

$$\begin{aligned} \overline{\langle (\Delta n_A)^2 \rangle}_{R,R} &= \sum_{p,p'} \overline{\langle \Delta n_p^R \Delta n_{p'}^R \rangle} (P_1 + 2 P_2)(P_1' + 2 P_2') + \\ &+ \sum_p \overline{\langle n_p^R \rangle} [P_1 + 4 P_2 - (P_1 + 2 P_2)^2]. \end{aligned} \quad (58)$$

A generalization of the results above to decays into more than two particles should be possible using similar arguments. A branching ratio b_r can be easily introduced by making $P_l \rightarrow b_r P_l$.

VI. RESULTS

Calculations within the above scheme can be directly implemented in a computer code, which enables us to calculate the variances and covariances of different particle multiplicities.

Our aim here is neither a direct comparison with experimental data nor a test of different signatures with realistic background contributions. We rather examine the effect of different kinds of limitations to simple fluctuation measures and compare analytical and simulation results. Our background models and resonance contributions are not meant to be complete, but exemplify how different effects may be implemented and how they affect fluctuations. For that reason, only the decay of ρ mesons into pions is considered.

Since the mass and the coupling of pions are better constrained, we concentrate on these particles. A general discussion on the limitations and advantages of our methods and results is presented in Sec. VII.

A. Signatures from pions

We now turn to signatures coming exclusively from charged pions and examine their dependence on the chiral correlation length ξ . As in Ref. [19], we use $T = 130$ MeV for the temperature of the system and $R_p = 6.8$ fm for its average radius. We choose to display results for the increase in the ratio between the variance and the average of the multiplicity of charged pions, relative to its value at ξ_r , as a function of ξ :

$$\text{Signal}(\xi) := \frac{V_{\pi_{ch}}(\xi)/M_{\pi_{ch}}(\xi)}{V_{\pi_{ch}}(\xi_r)/M_{\pi_{ch}}(\xi_r)} - 1, \quad (59)$$

where $M_{\pi_{ch}} = \overline{\langle N_{\pi_{ch}} \rangle}$ and $V_{\pi_{ch}} = \overline{\langle (\Delta N_{\pi_{ch}})^2 \rangle}$ are the mean and variance of the charged pion multiplicity and, unlike in Ref. [19], we use $\xi_r = 0.4$ fm $\sim 1/m_{\sigma}^{\text{vac}}$ as a baseline value for the correlation length. Figure 3 displays results for the effects of critical and background contributions as well as the decay of ρ mesons into two pions. These results suggest that the chosen signature would hardly reach $\sim 1\%$. Figures 4, 5, 6 and 7 show results for the signal at $\xi = 5 \xi_r = 2.0$ fm, S_5 , as a function of the lower transverse momentum cut p_- , the pseudo-rapidity cut η_C , a constant detector efficiency and the branching ratio for the decay of ρ mesons into two pions, respectively.

Figure 4 also presents simulation results, showing good agreement with analytical ones for different transverse momentum cuts. This validates the approximation, made in Sec. IV, that fluctuations of $F(p)$ are negligible. The decrease of S_5 with an increasing p_- is due to a larger concentration of pions at low transverse momentum, which also makes the value of the superior transverse momentum cut p_+ less relevant.

⁶ In this case, however, these probabilities are also affected by changes in the mass of the particles, driven by critical fluctuations.

Attention should be drawn to the fact that the signature in Eq. (59) is also affected by particle number fluctuations which are inherent to a grand-canonical ensemble. These fluctuations alone yield a nearly Poissonian contribution, $V_{\pi_{ch}}/M_{\pi_{ch}}|_{GC} \approx 1$, which dominates the variance of the particle multiplicity. Since our calculations only have meaning within a grand-canonical ensemble, this contribution is present in all of our results, even the ones for “pure” critical contributions. This is partly the reason why our signals grow more slowly in ξ than one would naively expect. While subtracting a Poissonian contribution from our signature would result in much stronger relative signals, such signals would correspond to much less impressive values in absolute numbers, signaling to small increases in the particle number fluctuations. On the other hand, calculating the signal with respect to the full background contributions, including the ones which are intrinsic to a grand-canonical ensemble, has the advantage of providing a direct comparison to a number we know is of order $\sim \mathcal{O}(1)$. The signals obtained after subtracting a Poissonian background are related to our results by an approximately constant ratio, which is different for each case in Fig. 3. Without the additional spurious fluctuations, this ratio is of roughly ~ 80 , but it drops to ~ 2.2 in their presence. If the decay of ρ mesons is included, these values drop to ~ 62 and ~ 1.7 , respectively. This shows that, despite growing more slowly with ξ , our naive signature is a lot more robust to other background contributions.

The behavior for different pseudorapidity cuts in Fig. 5 can be understood by arguments similar to the ones in Ref. [28], although, there, expansion effects are considered and background contributions are not contemplated. Because of the isotropy assumption, as a larger rapidity window is used, a larger number of pairs of momentum modes, roughly proportional to the square of the window in the cosine of the polar angle $[\Delta(\cos\theta)]^2$, is correlated by critical contributions. Since the results are normalized by the average multiplicity of charged pions ($\propto \Delta(\cos\theta)$), they scale roughly as $\propto \Delta(\cos\theta) \propto F(p) \propto \tanh\eta_C$ if p_T is unrestricted, as can also be seen from Eq. (40) and is confirmed by the very successful $a \tanh(\eta_C)$ fit to the results. Since the expansion of the system was not considered, the interpretation of these results is purely geometric.

The dependence of S_5 on the detector efficiency, shown in Fig. 6, can be modeled by assuming a detection probability proportional to the efficiency e , so that $V_{\pi_{ch}}/M_{\pi_{ch}} = \lambda(\xi)e + 1$ and S_5 takes the form

$$S_5 = \frac{\kappa e}{\gamma e + 1}, \quad (60)$$

which is in excellent agreement with results.⁷

⁷ Fits to the results yield $\kappa = (2.5107 \pm 0.0000003) 10^{-2}$, $\gamma = (1.25693 \pm 0.00001) 10^{-4}$ without background contributions and $\kappa = (2.36801 \pm 0.0000004) 10^{-2}$, $\gamma = (8.54053 \pm 0.0000004) 10^{-3}$ when taking them into account.

As for the dependence of the results on the branching ratio of the decay of a ρ meson into two pions, shown in Fig. 7, it can be roughly described by assuming a Poissonian distribution on the number of decay products, with a mean proportional to the branching ratio b_r . Combining contributions from decay products with critical ones while assuming statistical independence between the two and neglecting the dependence of $M_{\pi_{ch}}$ in ξ yields

$$S_5 = \frac{\chi}{\zeta b_r + 1}, \quad (61)$$

which can fit the results quite well.⁸

The signal in Fig. 3 scales quadratically with the correlation length, with a proportionality factor which depends mainly on the square of the coupling G in Eq. (4), as well as our models for spurious contributions and the chosen acceptance window. While the estimate of $G = 300$ MeV near the critical point carries large uncertainties related to medium effects and the properties of the σ meson, it is clear that it should be much smaller than in vacuum, by a factor of $\sim 1/6$. Since this estimate considers a vacuum sigma mass of 600 MeV, we believe it to be optimistic [9]. Regarding spurious contributions, while our models most likely overestimate the role of temperature fluctuations, they largely neglect the complex nature of heavy-ion collision experiments. Among others, the effect of indirect particles is underestimated, since we have only considered the decay of ρ mesons. Finally, although we rely on the the simplified interaction Lagrangian of Eq. (4), we believe it captures most of the physics, at least for second-order fluctuations. Further caveats to our results are discussed in Sec. VII.

VII. CONCLUDING REMARKS

In this paper, we have outlined a simple framework for calculating multiplicity fluctuations in the neighborhood of the QCD critical point. As we have shown, it allows for the introduction of general long-range fluctuations, acceptance cuts and resonance decay in a systematic way. Acceptance window effects were treated probabilistically, giving rise to extra contributions to fluctuations, and applied to resonance decay. Finite-size effects were also included, which could be important at low collision energies. Moreover, there is no reason one should not extrapolate results to the continuum limit.

While we have calculated simple signatures from Gaussian fluctuations of charged pions, the same treatment might as well be applied to the calculation of more interesting signatures, such as higher moments of the net-proton distribution. Nevertheless, the inclusion of other

⁸ Fits to the results yield $\chi = 2.45388 \pm 0.002523$, $\zeta = (2.59846 \pm 0.02242) 10^{-3}$ without background contributions and $\chi = 1.28827 \pm 0.00122$, $\zeta = (7.27304 \pm 0.02838) 10^{-3}$ when taking them into account.

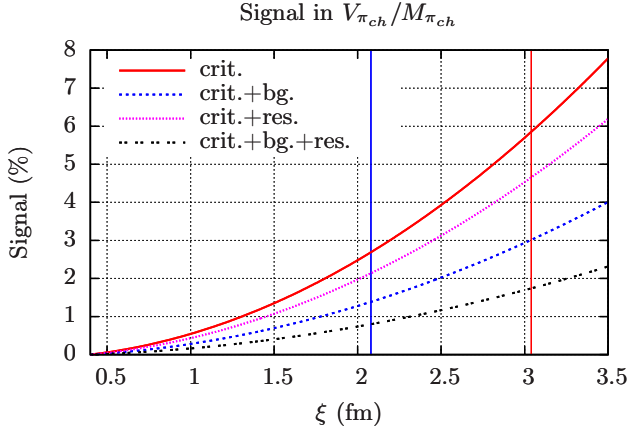


FIG. 3. Signal in the variance of the charged pion multiplicity $N_{\pi^+} + N_{\pi^-}$ scaled by its average value. Different curves correspond to results including (pure) critical contributions, background contributions (bg.) and/or the decay of ρ resonances into two pions (res.). The signal is displayed as a function of the correlation length at freeze-out, ξ , in relation to $\xi = \xi_r = 0.4$ fm, and the vertical lines correspond to the maximum possible values of ξ discussed in Sec. II A. Here, the acceptance window is fixed at $|\eta| < 0.5$ and $0.3 < p_T < 1$ GeV.

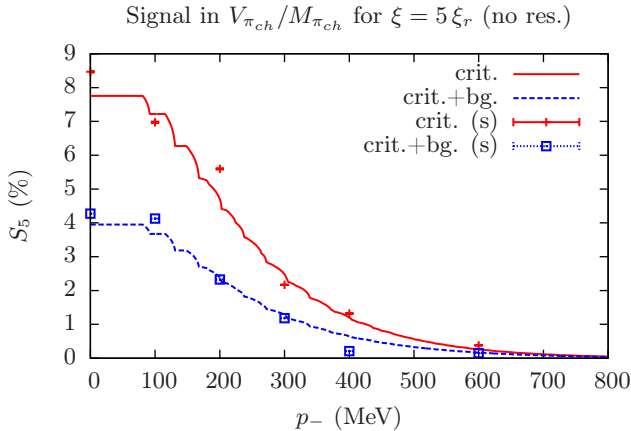


FIG. 4. Increase in the variance of the charged pion multiplicity $N_{\pi^+} + N_{\pi^-}$ scaled by its average value when the correlation length increases from $\xi_r = 0.4$ fm to $\xi_c = 2.0$ fm, as a function of the lower limit p_- to the transverse momentum p_T , both with and without background contributions (bg.). Curves represent analytic results while points show results from numeric simulations. The acceptance window is given by $|\eta| < 0.5$ and $p_- < p_T < 1$ GeV and contributions from resonance decay are not contemplated.

particles, as well as an extension to non-Gaussian fluctuations, requires the inclusion of poorly known parameters, such as the proton mass m_p and the proton coupling constant g near the critical point, and the parameters required for an appropriate description of non-Gaussian fluctuations [10], a problem which may be partially solved by somehow extracting information about fluctuations in

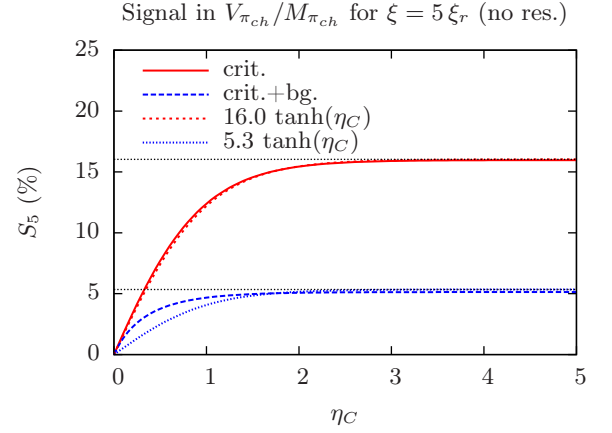


FIG. 5. Increase in the variance of the charged pion multiplicity $N_{\pi^+} + N_{\pi^-}$ scaled by its average value when the correlation length increases from $\xi_r = 0.4$ fm to $\xi_c = 2.0$ fm, as a function of the pseudorapidity cut η_C , both with and without background contributions (bg.), for $0 < p_T < 2$ GeV. Fits of the form $a \tanh(\eta_C)$ to the results are also shown. Contributions from resonance decay are not contemplated.

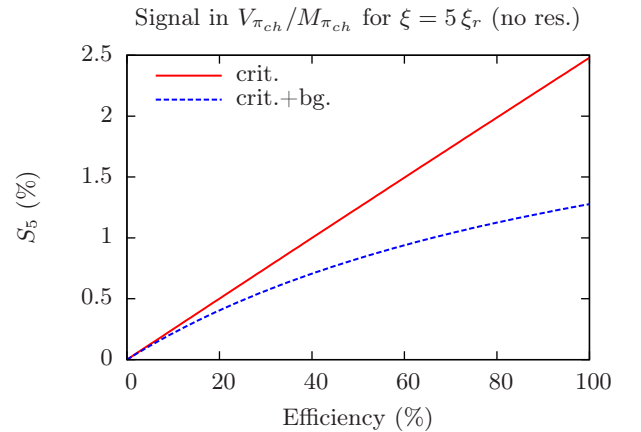


FIG. 6. Increase in the variance of the charged pion multiplicity $N_{\pi^+} + N_{\pi^-}$ scaled by its average value when the correlation length increases from $\xi_r = 0.4$ fm to $\xi_c = 2.0$ fm, as a function of a constant detector efficiency. Contributions from resonance decay are not contemplated. Results including background fluctuations (bg.) are also shown. The acceptance window is fixed at $|\eta| < 0.5$ and $0.3 < p_T < 1$ GeV and contributions from resonance decay are not contemplated.

equilibrium from a provided equation of state.

Our approach presents some important limitations. It includes no dynamics, except for the estimation of the maximum value of the correlation length, and no freeze-out mechanism or rescattering. Fluctuations of the σ_0 and other parameters are taken to be perfectly homogeneous and particles are assumed to obey perfect symmetry and excessively restrictive boundary conditions.

Moreover, our background fluctuations are still unredefined, although they could be easily substituted for more

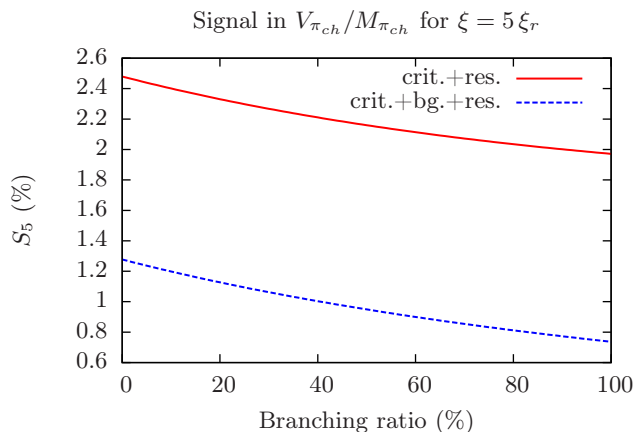


FIG. 7. Increase in the variance of the charged pion multiplicity $N_{\pi^+} + N_{\pi^-}$ scaled by its average value when the correlation length increases from $\xi_r = 0.4$ fm to $\xi_c = 2.0$ fm, as a function of a constant branching ratio for the decay of ρ mesons into two pions. Results including background fluctuations (bg.) are also shown. The acceptance window is fixed at $|\eta| < 0.5$ and $0.3 < p_T < 1$ GeV and contributions from resonance decay are not contemplated.

physically and experimentally motivated models. Information on the statistical distribution of thermodynamic parameters may be extracted from the event-by-event distribution of the mean transverse momentum of particles, specially for temperature fluctuations. In this case, different particle species, with different masses and charges, might be used to separate effects from temperature, chemical potential and volume fluctuations. In the case of volume fluctuations, a more complete model could be achieved by assigning a probability distribution for the proportionality factor C in Sec. II B.

A relevant restriction is that we assume isotropy and global equilibrium, neglecting the effects of flow. This means that our results for the acceptance window dependence should not be taken at face value, especially at large pseudorapidities (compare with [28]) and, even

so, their validity is limited to central collisions. Although these effects were not considered, they can be roughly included by using a prescribed velocity profile and writing

$$F(p) = \int \frac{d^3x}{V} \int_{\tilde{\Omega}_{\text{acc}}(p, \mathbf{x})} \frac{d\Omega}{4\pi}, \quad (62)$$

where $\tilde{\Omega}_{\text{acc}}(p, \mathbf{x})$ is the solid angle coverage of the acceptance window when boosted with the velocity of the fluid element at \mathbf{x} . This would, however, provide only a crude solution.

The methods we have employed seem to be very adaptable, enabling several effects to be considered at once in reasonably simple analytical calculations and simulations which are relatively cheap in computer power. These simulations produce integer numbers of particles without introducing artificial Poissonian noise and might be used to feed some kind of rescattering algorithm.

Another nice feature of our simulations is that they can be adapted to include global conservation laws (see, for instance Refs. [44, 46, 47]) by restricting them to configurations with fixed values for conserved quantities, discarding samples which do not follow this criterion. However, this would raise the computing time by increasing both the number of necessary samples and the number of considered momentum modes.

ACKNOWLEDGMENTS

The authors would like to thank V. Koch, M. Lisa, L. Moriconi, D. Parganlija, P. Sorensen, M. Tannenbaum and G. Torrieri for elucidative conversations and constructive criticism, and the organizers and participants of the INT Program “Exploring the QCD Phase Diagram through Energy Scans” for two weeks of very inspiring discussions and presentations. We thank the Institute for Nuclear Theory at the University of Washington for its hospitality and the Department of Energy for partial support during the completion of this work. We also acknowledge CNPq and FAPERJ for their financial support.

-
- [1] Y. Aoki, G. Endrodi, Z. Fodor, S. D. Katz, and K. K. Szabo, “The Order of the quantum chromodynamics transition predicted by the standard model of particle physics,” *Nature* **443**, 675–678 (2006), arXiv:hep-lat/0611014 [hep-lat].
 - [2] S. Borsanyi, G. Endrodi, Z. Fodor, A. Jakovac, S. D. Katz, S. Krieg, C. Ratti, and K. K. Szabo, “The QCD equation of state with dynamical quarks,” *JHEP* **11**, 077 (2010), arXiv:1007.2580 [hep-lat].
 - [3] M. A. Stephanov, “QCD phase diagram: An Overview,” *PoS LAT2006*, 024 (2006), arXiv:hep-lat/0701002 [hep-lat].
 - [4] M. A. Stephanov, “QCD phase diagram and the critical point,” *Prog.Theor.Phys.Suppl.* **153**, 139–156 (2004), arXiv:hep-ph/0402115 [hep-ph].
 - [5] K. Rajagopal, “The Chiral Phase Transition in Qcd: Critical Phenomena and Long Wavelength Pion Oscillations,” in *Quark-Gluon Plasma 2.*, edited by R. C. Hwa (World Scientific Publishing Co, 1995) pp. 484–554.
 - [6] X. Luo, “Exploring the QCD Phase Structure with Beam Energy Scan in Heavy-ion Collisions,” *Nucl. Phys.* **A956**, 75–82 (2016), arXiv:1512.09215 [nucl-ex].
 - [7] X. Luo (for the STAR Collaboration), “Energy Dependence of Moments of Net-Proton

- and Net-Charge Multiplicity Distributions at STAR,” PoS CPOD2014, 019 (2015), arXiv:1503.02558 [nucl-ex].
- [8] J. Xu (for the STAR Collaboration), “Energy Dependence of Moments of Net-Proton, Net-Kaon, and Net-Charge Multiplicity Distributions at STAR,” J. Phys. Conf. Ser. **736**, 012002 (2016), arXiv:1611.07134 [hep-ex].
- [9] M. A. Stephanov, K. Rajagopal, and E. V. Shuryak, “Event-by-event fluctuations in heavy ion collisions and the QCD critical point,” Phys. Rev. D **60**, 114028 (1999), arXiv:hep-ph/9903292 [hep-ph].
- [10] M.A. Stephanov, “Non-Gaussian fluctuations near the QCD critical point,” Phys. Rev. Lett. **102**, 032301 (2009), arXiv:0809.3450 [hep-ph].
- [11] C. Athanasiou, K. Rajagopal, and M. Stephanov, “Using Higher Moments of Fluctuations and their Ratios in the Search for the QCD Critical Point,” Phys. Rev. D **82**, 074008 (2010), arXiv:1006.4636 [hep-ph].
- [12] B. Berdnikov and K. Rajagopal, “Slowing out-of-equilibrium near the QCD critical point,” Phys. Rev. D **61**, 105017 (2000), arXiv:hep-ph/9912274 [hep-ph].
- [13] J. Braun, B. Klein, H. J. Pirner, and A. H. Rezaeian, “Volume and quark mass dependence of the chiral phase transition,” Phys. Rev. D **73**, 074010 (2006), arXiv:hep-ph/0512274 [hep-ph].
- [14] O. Kiriya, T. Kodama, and T. Koide, “Finite-size effects on the QCD phase diagram,” (2006), arXiv:hep-ph/0602086 [hep-ph].
- [15] L. F. Palhares, E. S. Fraga, and T. Kodama, “Chiral transition in a finite system and possible use of finite size scaling in relativistic heavy ion collisions,” J. Phys. G **38**, 085101 (2011), arXiv:0904.4830 [nucl-th].
- [16] E. S. Fraga, L. F. Palhares, and P. Sorensen, “Finite-size scaling as a tool in the search for the QCD critical point in heavy ion data,” Phys. Rev. C **84**, 011903 (2011), arXiv:1104.3755 [hep-ph].
- [17] S. Mukherjee, R. Venugopalan, and Y. Yin, “Real time evolution of non-Gaussian cumulants in the QCD critical regime,” Phys. Rev. C **92**, 034912 (2015), arXiv:1506.00645 [hep-ph].
- [18] S. Mukherjee, R. Venugopalan, and Y. Yin, “Universal off-equilibrium scaling of critical cumulants in the QCD phase diagram,” Phys. Rev. Lett. **117**, 222301 (2016), arXiv:1605.09341 [hep-ph].
- [19] Maurício Hippert, Eduardo S. Fraga, and Edivaldo M. Santos, “Critical versus spurious fluctuations in the search for the QCD critical point,” Phys. Rev. D **93**, 014029 (2016), [Phys. Rev. D **93**, 014029 (2016)], arXiv:1507.04764 [hep-ph].
- [20] M. Gorenstein, “New Theoretical Results on Event-by-Event Fluctuations,” PoS CPOD2014, 017 (2015), arXiv:1505.04135 [nucl-th].
- [21] N. R. Sahoo, S. De, and T. K. Nayak, “Baseline study for higher moments of net-charge distributions at energies available at the BNL Relativistic Heavy Ion Collider,” Phys. Rev. C **87**, 044906 (2013), arXiv:1210.7206 [nucl-ex].
- [22] C. Herold, M. Nahrgang, Y. Yan, and C. Kobdaj, “Dynamical net-proton fluctuations near a QCD critical point,” Phys. Rev. C **93**, 021902 (2016), arXiv:1601.04839 [hep-ph].
- [23] X. Luo, Ji Xu, B. Mohanty, and N. Xu, “Volume fluctuation and auto-correlation effects in the moment analysis of net-proton multiplicity distributions in heavy-ion collisions,” J. Phys. G **40**, 105104 (2013), arXiv:1302.2332 [nucl-ex].
- [24] N. G. Antoniou, F. K. Diakonou, and E. N. Saridakis, “Evolution of Critical Correlations at the QCD Phase Transition,” Nucl. Phys. A **784**, 536 (2007), arXiv:hep-ph/0610382 [hep-ph].
- [25] N. G. Antoniou, F. K. Diakonou, and E. N. Saridakis, “Evolutionary intermittency and the QCD critical point,” Phys. Rev. C **78**, 024908 (2008), arXiv:0709.0339 [hep-ph].
- [26] M. A. Stephanov, “Evolution of fluctuations near QCD critical point,” Phys. Rev. D **81**, 054012 (2010), arXiv:0911.1772 [hep-ph].
- [27] A. Bzdak and V. Koch, “Acceptance corrections to net baryon and net charge cumulants,” Phys. Rev. C **86**, 044904 (2012), arXiv:1206.4286 [nucl-th].
- [28] B. Ling and M. A. Stephanov, “Acceptance dependence of fluctuation measures near the QCD critical point,” Phys. Rev. C **93**, 034915 (2016), arXiv:1512.09125 [nucl-th].
- [29] M. Gell-Mann and M. Levy, “The axial vector current in beta decay,” Nuovo Cim. **16**, 705 (1960).
- [30] J. Zinn-Justin, “Determination of critical exponents and equation of state by field theory method,” *Proceedings of the 6th International Conference, PI’98 - 6th International Conference on Path integrals from PeV to TeV: 50 years after Feynman’s paper.*, Florence, Italy, August 25-29, 1998, arXiv:hep-th/9810193 [hep-th].
- [31] R. Guida and J. Zinn-Justin, “3-D Ising model: The Scaling equation of state,” Nucl. Phys. B **489**, 626–652 (1997), arXiv:hep-th/9610223 [hep-th].
- [32] P. C. Hohenberg and B. I. Halperin, “Theory of Dynamic Critical Phenomena,” Rev. Mod. Phys. **49**, 435–479 (1977).
- [33] X. Luo and N. Xu, “Search for the QCD Critical Point with Fluctuations of Conserved Quantities in Relativistic Heavy-Ion Collisions at RHIC : An Overview,” Nucl. Sci. Tech. **28**, 112 (2017), arXiv:1701.02105 [nucl-ex].
- [34] H. De Vries, C. W. De Jager, and C. De Vries, “Nuclear charge-density-distribution parameters from elastic electron scattering,” At. Data Nucl. Data Tables **36**, 495 (1987).
- [35] C.W. De Jager, H. De Vries, and C. De Vries, “Nuclear charge- and magnetization-density-distribution parameters from elastic electron scattering,” At. Data Nucl. Data Tables **14**, 479 (1974).
- [36] V. Skokov, B. Friman, and K. Redlich, “Volume Fluctuations and Higher Order Cumulants of the Net Baryon Number,” Phys. Rev. C **88**, 034911 (2013), arXiv:1205.4756 [hep-ph].
- [37] M. I. Gorenstein and M. Gazdzicki, “Strongly Intensive Quantities,” Phys. Rev. C **84**, 014904 (2011), arXiv:1101.4865 [nucl-th].

- [38] F. Karsch, K. Morita, and K. Redlich, “Effects of kinematic cuts on net-electric charge fluctuations,” *Phys. Rev. C* **93**, 034907 (2016), arXiv:1508.02614 [hep-ph].
- [39] P. Garg, D. K. Mishra, P. K. Netrakanti, B. Mohanty, A. K. Mohanty, B. K. Singh, and N. Xu, “Conserved number fluctuations in a hadron resonance gas model,” *Phys. Lett. B* **726**, 691–696 (2013), arXiv:1304.7133 [nucl-ex].
- [40] C. Pruneau, S. Gavin, and S. Voloshin, “Methods for the study of particle production fluctuations,” *Phys. Rev. C* **66**, 044904 (2002), arXiv:nucl-ex/0204011 [nucl-ex].
- [41] M. Bluhm, M. Nahrgang, S. A. Bass, and T. Schaefer, “Impact of resonance decays on critical point signals in net-proton fluctuations,” *Eur. Phys. J. C* **77**, 210 (2017), arXiv:1612.03889 [nucl-th].
- [42] D. K. Mishra, P. Garg, P. K. Netrakanti, and A. K. Mohanty, “Effect of resonance decay on conserved number fluctuations in a hadron resonance gas model,” *Phys. Rev. C* **94**, 014905 (2016), arXiv:1607.01875 [hep-ph].
- [43] M. Nahrgang, M. Bluhm, P. Alba, R. Bellwied, and C. Ratti, “Impact of resonance regeneration and decay on the net-proton fluctuations in a hadron resonance gas,” *Eur. Phys. J. C* **75**, 573 (2015), arXiv:1402.1238 [hep-ph].
- [44] V. V. Begun, M. I. Gorenstein, M. Hauer, V. P. Konchakovski, and O. S. Zozulya, “Multiplicity Fluctuations in Hadron-Resonance Gas,” *Phys. Rev. C* **74**, 044903 (2006), arXiv:nucl-th/0606036 [nucl-th].
- [45] S. Jeon and V. Koch, “Fluctuations of particle ratios and the abundance of hadronic resonances,” *Phys. Rev. Lett.* **83**, 5435–5438 (1999), arXiv:nucl-th/9906074 [nucl-th].
- [46] A. Bzdak, V. Koch, and V. Skokov, “Baryon number conservation and the cumulants of the net proton distribution,” *Phys. Rev. C* **87**, 014901 (2013), arXiv:1203.4529 [hep-ph].
- [47] V. V. Begun, M. Gazdzicki, M. I. Gorenstein, and O. S. Zozulya, “Particle number fluctuations in canonical ensemble,” *Phys. Rev. C* **70**, 034901 (2004), arXiv:nucl-th/0404056 [nucl-th].